



1

2

3

4

5

6

What Fraction of the Pacific and Indian Oceans' Deep Water is formed in the North Atlantic?

7

8

9

10

11

12

13

14

15

16

17

James W.B. Rae
School of Earth & Environmental Sciences
Irvine Building
University of St. Andrews
St. Andrews
KY16 9AL
UK
jwbr@st-andrews.ac.uk

18

19

20

21

22

23

24

25

Wally Broecker
Lamont-Doherty Earth Observatory of Columbia University
61 Route 9W/PO Box 1000
Palisades, NY 10964
broecker@ldeo.columbia.edu; (845) 365-8413 tel; (845) 365-8169 fax

26

27

28

29

30

31

32

33

34

Contribution to the
Ernst Maier-Reimer Volume



35 **Abstract**

36 In this contribution we explore constraints on the fractions of deep water present in
37 Indian and Pacific Oceans which originated in the northern Atlantic and in the Southern Ocean.
38 Based on PO_4^* we show that if ventilated Antarctic shelf waters characterize the Southern
39 contribution, then the proportions are close to 50-50. If instead a Southern Ocean bottom water
40 value is used, the Southern contribution is increased to 75 %. While this larger estimate may
41 characterize the volume of water entering the Indo-Pacific from the Southern Ocean, it contains a
42 significant portion of entrained northern water. We also note that ventilation may be highly
43 tracer dependent: for instance Southern Ocean waters may contribute only 35% of the deep
44 radiocarbon budget, even if their volumetric contribution is 75%. In our estimation, the most
45 promising approaches involve using CFC-11 to constrain the amount of deep water formed in the
46 Southern Ocean.



47

48 **Remembering Ernst (W.B.)**

49 In 1987, Klaus Hasselmann was invited to Lamont-Doherty to present three lectures on
50 climate. The first two dealt with what he referred to as PIPS and POPS. They didn't ring my bell.
51 But the third one hit home. In it Klaus laid out the distribution of properties generated by Ernst
52 Maier-Reimer's ocean circulation model (Maier-Reimer & Hasselmann, 1987). I was particularly
53 interested in its ability to reproduce the distribution of natural radiocarbon in the ocean. But the
54 plots he showed were at first look incomprehensible. It turned out, that rather than presenting
55 differences from the ^{14}C to C ratio in atmospheric CO_2 , they were referenced to that in mean
56 ocean water. After the lecture, I offered to come to Hamburg to help Maier-Reimer switch to a
57 mode of presentation understandable to those conversant with the ^{14}C measurements. And so it
58 was I spent three weeks with Ernst probing not only the ^{14}C to C distribution produced by his
59 model, but also that of O_2 and SiO_2 . For me it was a fantastic learning experience. Not only did
60 Ernst have an amazing mind but he had a knack of teaching by tweaking his model. Thus began
61 a lasting collaboration and friendship.

62

63 **PO_4^***

64 This led to an interest in determining the contributions of NADW and AABW to the
65 ventilation of the deep Pacific and Indian Oceans. As the ratio of O_2 utilization to PO_4 release
66 during respiration appears to be nearly constant throughout the ocean's interior (Takahashi et al.
67 1985; Anderson & Sarmiento, 1994), Broecker and colleagues (Broecker et al., 1985, Broecker
68 et al., 1998) proposed a conservative property PO_4^* :

$$69 \quad \text{PO}_4^* = \text{PO}_4 + \frac{\text{O}_2}{175} - 1.95 \mu\text{mol/kg}.$$

70 As only differences between PO_4^* values are of importance, the choice of the constant 1.95 is
71 arbitrary. Hence zero would have been more convenient. Other choices for the O_2 consumption
72 to PO_4 remineralisation ratio are also possible (Hupe & Karstensen, 2000), but have little impact



73 on our global-scale calculations, so we stick with the formulation of Broecker et al. (1998)
74 above.

75 The attraction of PO_4^* as a water mass tracer is that although the deep waters formed in
76 the northern Atlantic range widely in temperature, all the contributors have PO_4^* values close to
77 0.7 (Figure 1). Further, the deep waters (i.e., >2000 m) in the deep Pacific and Indian Oceans
78 have PO_4^* values close to 1.4. Hence were the PO_4^* for deep waters formed in the Southern
79 Ocean known, the relative amounts of deep water produced in the two source regions could be
80 established.

81 Based on PO_4^* , Broecker et al. (1998) concluded that the deep Pacific and Indian Oceans
82 received about half of their water from the northern Atlantic and half from the Southern Ocean.
83 However, Johnson (2008), Gebbie and Huybers (2010), and Khatiwala et al. (2012), using more
84 complex inversions of multiple tracers, concluded that only about one quarter of this water came
85 from the northern Atlantic. If the ~16 Sverdrups of NADW (Broecker et al. 1998; Ganachaud &
86 Wunch, 2000; Smethie and Fine, 2001) account for only one quarter of the water ventilating the
87 Indian and Pacific Ocean, then the Southern Ocean must supply about 48 Sverdrups. On the
88 other hand, if half the deep water ventilating the deep sea were produced in the northern Atlantic,
89 then the required Southern Ocean ventilation flux would be reduced to about 16 Sverdrups. Quite
90 a difference!

91

92 **PO_4^* calculations revisited**

93 Based on the GLODAPv2 dataset (Key et al., 2015; Olsen et al., 2016) we have re-
94 examined deep ocean PO_4^* distributions. The mean PO_4^* value for deep (>2000 m) Indo-Pacific
95 waters (Figure 2) is 1.42 ± 0.04 (1 SD). We select waters below 2000 m as all determinations
96 (Johnson, 2008; Gebbie and Huybers, 2010; Khatiwala et al., 2012) suggest that these depths are
97 predominantly a two-component mixture of deep North Atlantic and Southern Ocean waters. To
98 help identify recently ventilated dense waters we also examined CFC11 and neutral density. The
99 mean PO_4^* value for deep (>1500 m) recently ventilated (CFC11>0.5 pmol/kg) waters in the



100 North Atlantic (Figure 2) is 0.74 ± 0.05 . These Indo-Pacific and Atlantic end-members are
101 within error of Broecker et al. (1998)'s values (1.39 and 0.73 respectively) and are relatively
102 insensitive to choice of geographical boundaries, depth, CFC, and density limits.

103 Determining the PO_4^* end member of Southern Ocean deep waters is less
104 straightforward. Broecker et al. (1998) use a PO_4^* value of 1.95. This value was obtained both
105 by extrapolating the $\text{PO}_4^* - \Theta$ relationship to the freezing point of sea water (Figure 1) and from
106 direct observations of sinking surface waters in the Weddell and Ross Seas (Figure 3). The 1.95
107 PO_4^* value is achieved if water upwelling in the Southern Ocean is cooled to the freezing point,
108 has about 65 percent of its O_2 deficiency replenished and loses little of its PO_4 to sinking
109 organics (see Table 1).

110 However while PO_4^* values of 1.95 characterize well-ventilated Antarctic shelf waters,
111 these entrain up to three times their volume in circumpolar deep water as they cascade down the
112 continental slope (Carmack & Foster, 1975; Orsi et al., 1999); indeed PO_4^* beautifully highlights
113 this process (Figure 3). As a result, by the time Antarctic bottom water enters the ACC it has
114 much lower PO_4^* : Weddell Sea bottom waters have PO_4^* of ~ 1.8 , and deep Ross Sea waters
115 ~ 1.6 (Figures 3 & 4). This basinal difference may be attributed to less input of NADW-
116 influenced circumpolar deep water and higher local ventilation rates in the Weddell Sea,
117 elevating PO_4^* in this more enclosed basin. The average circumpolar PO_4^* for recently
118 ventilated (CFC-11 > 0.5 pmol/kg) waters that have made it off the Antarctic shelf (> 1500 m) and
119 have neutral density higher than any North Atlantic waters (> 28.3 kg/m³) is 1.64 ± 0.07 (1 SD;
120 Figures 4 & 5).

121 Repeating Broecker et al.'s PO_4^* mass balance calculation with the Southern Ocean
122 bottom water value of 1.65 suggests that the deep Indo-Pacific is filled by 75 % Southern-
123 sourced water and 25 % NADW, with an uncertainty of $\pm 9\%$ (1 SD). This is within error of the
124 values obtained by Johnson (2008), Gebbie and Huybers (2010) and Khatiwala et al. (2012).
125 However if we use the well-ventilated shelf water value of 1.95, the north-south balance is closer
126 to 50:50 (Broecker et al. 1998). This highlights that while the volume flux of what are typically



127 considered southern deep waters into the Indo-Pacific may substantially outweigh that of
128 NADW, much of this water is entrained in the subsurface and does not reflect full Southern
129 Ocean ventilation.

130 Differences in the extent to which the Southern Ocean end member is locally ventilated
131 may thus explain much of the difference between the north-south balance obtained by Broecker
132 et al. (1998) versus Johnson (2008), Gebbie & Huybers (2010), and Khatiwala et al. (2010).
133 Johnson (2008) uses bottom water end member values for AABW, so it is unsurprising that our
134 estimates using a Southern Ocean bottom water value are similar to his. Gebbie & Huybers
135 (2008) and Khatiwala et al. (2010) use surface mixed layer conditions south of the ACC (Orsi et
136 al., 1995), taken from gridded climatologies (WOA, Conkright et al., 1994; WOCE, Gouretski &
137 Koltermann, 2004). As discussed by Gebbie & Huybers (2010), gridded data struggles to
138 capture shelf features and dense overflow waters, and thus excludes the end member values most
139 characteristic of the ventilated Southern Ocean interior (Warren 1981). High adiabatic upwelling
140 rates (Toggweiler & Samuels, 1995; Marshall & Speer, 2012) and deep mixed layers (Gordon &
141 Huber 1990; Dong et al., 2008) may also lead to inclusion of upwelled northern waters in these
142 Southern end members, despite little property modification in the Southern Ocean surface.
143 These issues may explain why the southern proportions of Gebbie & Huybers (2008) and
144 Khatiwala et al. (2010) are larger than those using the ventilated PO_4^* end member (as in
145 Broecker et al., 1998) and lie close to our estimates using bottom water values.

146 At the heart of this discussion lies the issue of what “counts” as ventilated Southern
147 water. Implicit in the Gebbie & Huybers (2008) and Khatiwala et al. (2010) studies is that any
148 waters reaching the Southern Ocean mixed layer may be considered Southern Ocean waters.
149 However these waters may experience little equilibration with Antarctic surface conditions,
150 including cooling, gas exchange, and nutrient use, depending on their transit time through the
151 Southern Ocean surface and the relaxation time of the tracer of interest. Therefore while they
152 may count in volume fluxes from the Southern Ocean (Talley 2013; Marshall & Speer 2012;
153 Lumpkin & Speer 2007), they may only partially reflect the exchanges of heat and CO_2 key to



154 the Southern Ocean's role in climate (Stocker & Johnsen 2003; Marinov et al., 2006; Barker et
155 al., 2009; Sigman et al., 2010; Ferrari et al. 2014).

156

157 **Ventilation Timescales and the Radiocarbon Budget**

158 The difference between Southern Ocean water mass volume and tracer ventilation is
159 particularly pronounced in the deep radiocarbon budget. Of the 220 moles per year of ^{14}C
160 undergoing radiodecay in the deep sea, about 20 moles/yr are resupplied by particle rain. As 16
161 Sverdrups of NADW supply about 130 moles $^{14}\text{C}/\text{yr}$, this leaves about 70 to be supplied from the
162 Southern Ocean (see Table 2). Ventilation of radiocarbon is thus dominated by the North
163 Atlantic, even if the Southern Ocean contributes greater volume. This is due to ^{14}C 's long
164 equilibration time and the limited exchange time between Southern Ocean surface waters and the
165 atmosphere. Waters upwelled into the surface thus do not reach equilibrium for ^{14}C and
166 radiocarbon gradients between surface and deep waters are very small (Broecker et al. 1985).
167 This, along with the presence of ^{14}C produced by H-bomb testing, also introduces large
168 uncertainty into any attempt to use radiocarbon to quantify the contribution of Southern Ocean
169 waters to the deep Indo-Pacific. The importance of northern versus southern ventilation may
170 thus depend on the tracer and process of interest.

171

172 **Constraints Based on CFCs**

173 Further insights into SO ventilation may be obtained using CFC data. As with ^{14}C , the
174 degree of surface water saturation (Schlosser et al., 1991) must be carefully considered if the
175 input flux of CFC tracer is to be converted to a ventilation flux for southern ocean water volume
176 (England et al., 1994). However CFCs have the advantages over ^{14}C of a much larger surface to
177 deep gradient and faster and less complicated equilibration. CFC-based estimates of the flux of
178 ventilated Southern Ocean water give values of ~ 15 Sv (Orsi et al., 2002; Schlitzer 2007). This
179 is similar to values for net production of NADW (Broecker et al., 1998; Ganachaud & Wunsch,
180 2000; Smethie & Fine, 2001), so appears to support roughly equal ventilation of the deep Indo-



181 Pacific between the northern Atlantic and the Southern Ocean (Broecker et al., 1998; Peacock et
182 al., 2000; Orsi et al., 2001). However this does not rule out a much higher water flux from the
183 south (Sloyan & Rintoul, 2001; Lumpkin & Speer, 2007; Talley 2013) – just not full equilibrium
184 with Southern Ocean surface conditions. We also note that if diffusion down isopycnals in the
185 open Southern Ocean is an important contributor to regional ventilation (Abernathy & Ferreira,
186 2015), this may not be as easily picked up as the CFC signal in shelf waters (Figure 5). The
187 reason is that low CFC-11 concentrations in a large volume may match high CFC-11
188 concentrations in a small volume.

189

190 **PO₄^{*} and the overturning circulation**

191 PO₄^{*} sections, surfaces, and tracer-tracer plots (Figures 7-9 and Supplementary Figures
192 1-6) also highlight patterns of circulation and mixing in the deep ocean. As can be seen, low
193 PO₄^{*} water from the North Atlantic mixes with high PO₄^{*} water formed in the Southern Ocean.
194 This mixing occurs along shared isopycnals in the ACC (Figure 8; Abernathy & Ferreira, 2015),
195 over rough seafloor topography (Naveira Garabato et al., 2004; Roemmich et al., 2009), and in
196 the deep surface mixed layer of the Southern Ocean (Gordon & Huber 1990; Dong et al., 2008).
197 These mixing patterns are also well illustrated on cross plots of PO₄^{*} with salinity and potential
198 temperature (Figures 9 and A1-3). NADW is identifiable as a salinity and PO₄^{*} maximum
199 sandwiched between fresher and higher PO₄^{*} southern waters above and below. By the time
200 circumpolar deep waters reach the Drake Passage, they have been somewhat homogenised,
201 though a PO₄^{*} minimum at mid-depths remains, tracing the persistent influence of North Atlantic
202 waters (Figure 7).

203 Other features of interest that are well highlighted by PO₄^{*} include: the input of very low
204 PO₄^{*} deep water from the Mediterranean Sea into mid-depths of the North Atlantic (Figure 8 &
205 A4); the penetration of relatively high PO₄^{*} water with a strong southern influence into the deep
206 NE Atlantic (Figure 8, A1, A6); and the formation of mid-depth circumpolar deep waters
207 represented by a PO₄^{*} maxima, slightly underlying the salinity minimum of AAIW. Intermediate



208 waters themselves are less readily identified by PO_4^* , forming in frontal regions with large
209 nutrient gradients (Talley, 1993; Talley, 1996; Sarmiento et al., 2004), and are better traced by
210 salinity (Figures 9, A1-3). Pacific deep waters returning through the Drake Passage are also hard
211 to identify using PO_4^* , falling in the middle of a PO_4^* mixing gradient between northern and
212 southern waters (Figures 8), and are better identified by their low oxygen and high silicate
213 (Figures A3, A5, A6).

214

215 **Conclusions**

216 The use of PO_4^* to constrain the northern and southern contributions to the waters in the
217 deep Indian and Pacific Oceans is highly dependent on the Southern Ocean end member value.
218 Using end members characterizing ventilated Antarctic shelf waters versus Southern Ocean deep
219 waters brackets the NADW contribution to between 50 and 25 % respectively. There is value to
220 both of these estimates: 75:25 may best characterize the ratio of deep Southern Ocean to North
221 Atlantic water volume, while 50:50 better represents the fluxes of well-ventilated waters, as
222 supported by CFC input models. In other words a large volume of the ocean's water experiences
223 some degree of exposure to the Southern Ocean surface, but the volume of those taking on a
224 more completely ventilated Southern Ocean signal is much smaller.

225

226

227



228

229

230

231

232

233

234

235

Table 1. Expected PO₄^{*}

236

237

Upwelled PO₄ = 2.2 μmol/kg

238

Upwelled O₂ = 210 μmol/kg

239

Saturation O₂ = 360 μmol/kg

240

241

Assume

242

1) No PO₄ utilization

243

2) 65% O₂ resaturation

244

245

Then

246

$$PO_4^* = 2.2 + \frac{0.65(360-210)+210}{175} - 1.95 = 1.95 \mu\text{mol/kg}$$

247


Table 2. Example ^{14}C budget for ~25% NADW contribution.

Loss via Radiodecay	
Volume of deep sea	$8 \times 10^{17} \text{ m}^3$
Mean ΣCO_2	2.3 moles/ m^3
Mean $\Delta^{14}\text{C}$	-175‰
Mean $^{14}\text{C}/\text{C}$	1.0×10^{-12}
Amount of ^{14}C in deep sea	1.8×10^6 moles
Amount decaying	220 moles/yr
Gain of Radiocarbon from North Atlantic	
Flux	16 Sverdrups
Flux	$6 \times 10^{14} \text{ m}^3/\text{yr}$
ΣCO_2	2.1 moles/ m^3
$\Delta^{14}\text{C}$	-67‰
$^{14}\text{C}/\text{C}$ - $^{14}\text{C}/\text{C}$ mean deep sea	0.13×10^{-12}
Input ^{14}C to deep sea	130 moles/yr
Gain of Radiocarbon from Southern Ocean	
Flux	45 Sverdrups
Flux	$17 \times 10^{14} \text{ m}^3/\text{yr}$
ΣCO_2	2.2 moles/yr
$\Delta^{14}\text{C}$	-154‰
$^{14}\text{C}/\text{C}$ - $^{14}\text{C}/\text{C}$ mean deep sea	0.025×10^{-12}
Input ^{14}C to deep sea	70 moles/yr
Gain of Radiocarbon by Particle Flux	
Carbon flux	$0.5 \text{ moles}/\text{m}^2/\text{yr}$
$\Delta^{14}\text{C}$	-70‰
$^{14}\text{C}/\text{C}$ - $^{14}\text{C}/\text{C}$ mean deep sea	0.126×10^{-12}
Input ^{14}C to deep sea	20 moles/yr
Total Gain of Radiocarbon	220 moles/yr

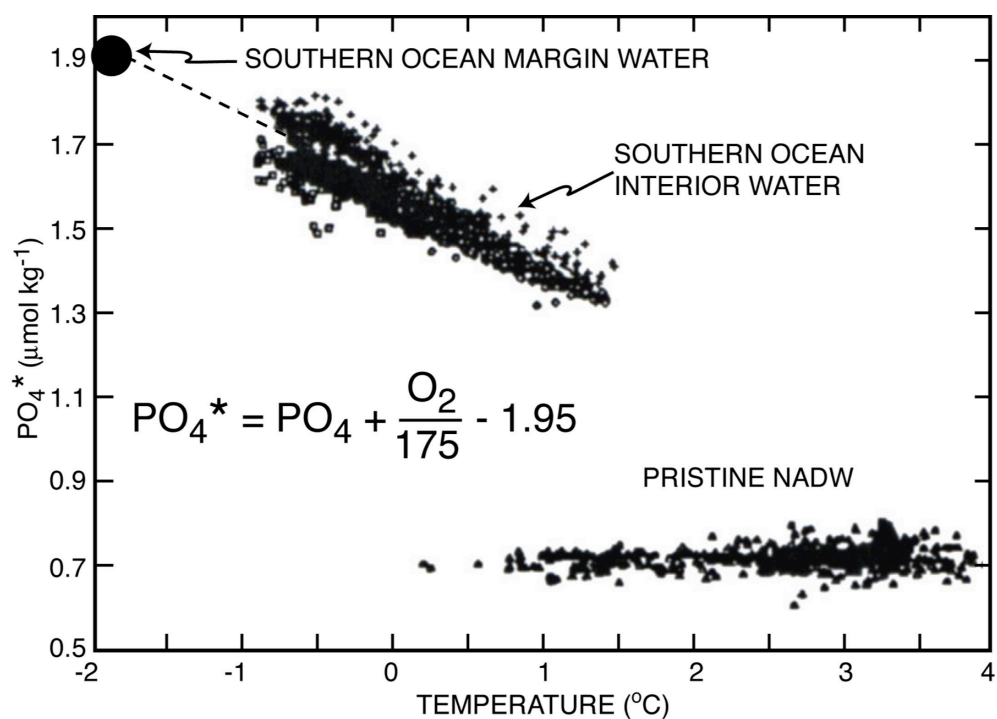


Figure 1. Plots of PO_4^* versus potential temperature for water formed in the northern Atlantic and in the Southern Ocean (based on measurements made as part of the GEOSECS expeditions). Note that all contributors of NADW have PO_4^* values within the measurement error of $0.75 \mu\text{mol/kg}$. The Southern Ocean PO_4^* was originally obtained by extrapolating the observed PO_4^* - temperature trend to sea water's freezing point (Table 1). As shown in Figures 3 and 4, this extrapolated value is consistent with values observed close to the Antarctic margin in the Weddell Sea.

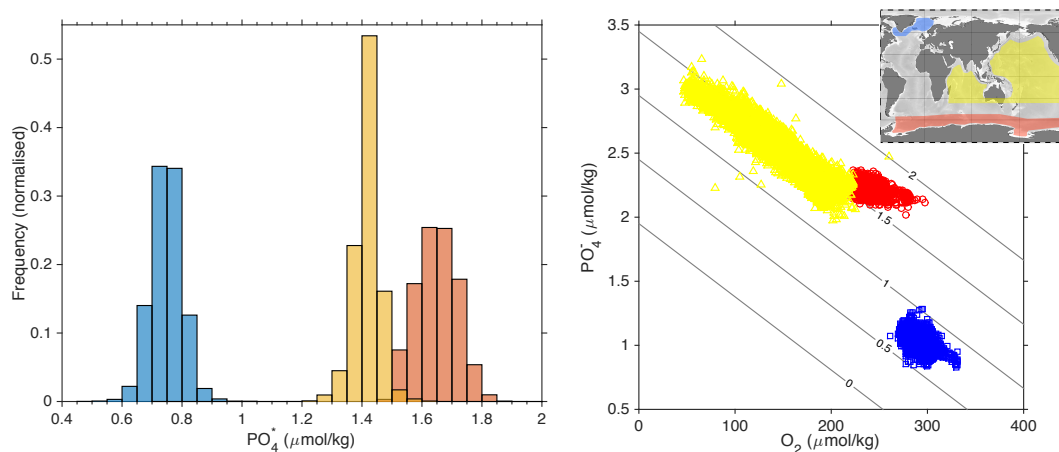


Figure 2: End member PO_4^* values for deep North Atlantic waters (blue) and deep Southern Ocean waters (red), along with deep Indo-Pacific waters (yellow). Data are from GLODAPv2 (Key et al., 2015; Olsen et al., 2016) and taken from the regions shown in the inset map. North Atlantic data are >1500 m and have $CFC_{11}>0.5$ pmol/kg; Southern Ocean data are >1500 m, have $CFC_{11}>0.5$ pmol/kg, and neutral density >28.3 kg/m^3 (see Figure 4); Indo-Pacific data are >2000 m. Normalised histograms of PO_4^* are shown for each region in the left hand panel, and the corresponding O_2 and PO_4^* concentrations on the right, contoured with PO_4^* .

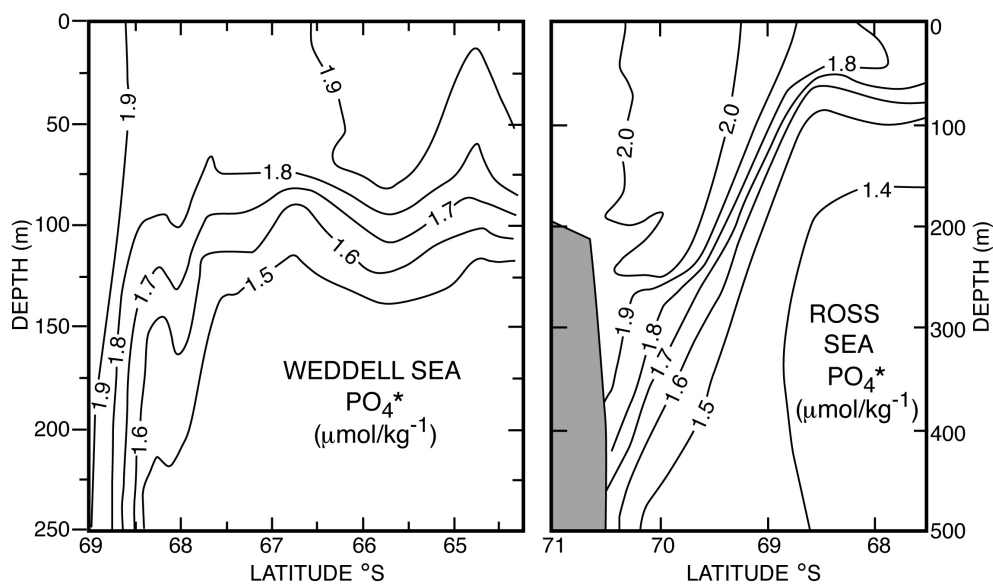


Figure 3. PO_4^* sections extending out from the Antarctic continent for the Weddell and Ross Seas. As can be seen, water with a value close to 1.95 is descending in a narrow margin-hugging plume.

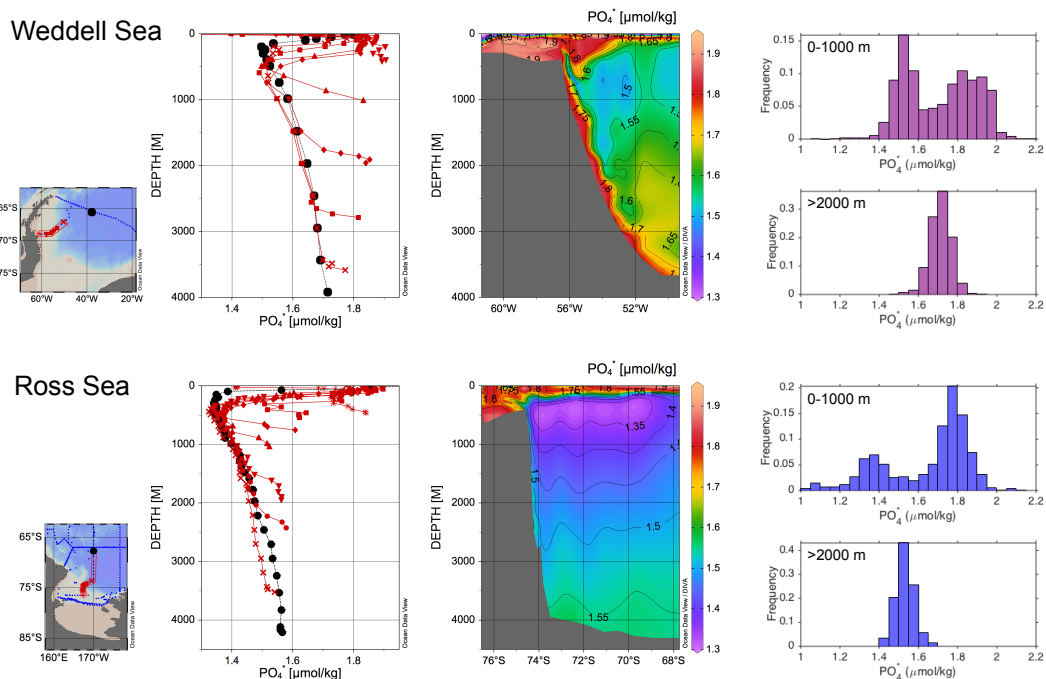


Figure 4: PO_4^* data in the Weddell and Ross Seas from the GLODAPv2 database. Sections (central panel) show high PO_4^* values on the shelves, that descend the continental margin in a narrow plume (Warren 1981). This is also picked out by selected depth profiles along these sections (left hand panel), with the black dots showing a profile further out from the shelf edge. Entrainment of low PO_4^* waters in the subsurface reduces southern deep water PO_4^* , from 1.95 on the shelf to ~ 1.65 at depth. This can also be seen in the histograms in the right hand panel (encompassing larger areas than those shown in the maps and sections), which show two distinct PO_4^* populations in the top 1000 m, which mix to give the more homogenous values at depth. Note that Weddell Sea waters have higher PO_4^* than Ross Sea waters, likely due to less influence of low- PO_4^* NADW and higher local deep water formation rates, elevating PO_4^* throughout this more enclosed basin. Data are from GLODAPv2 (Key et al., 2015; Olsen et al., 2016) with profiles, maps, and sections plotted in ODV (Schlitzer 2015), with sections contoured using isopycnal gridding.

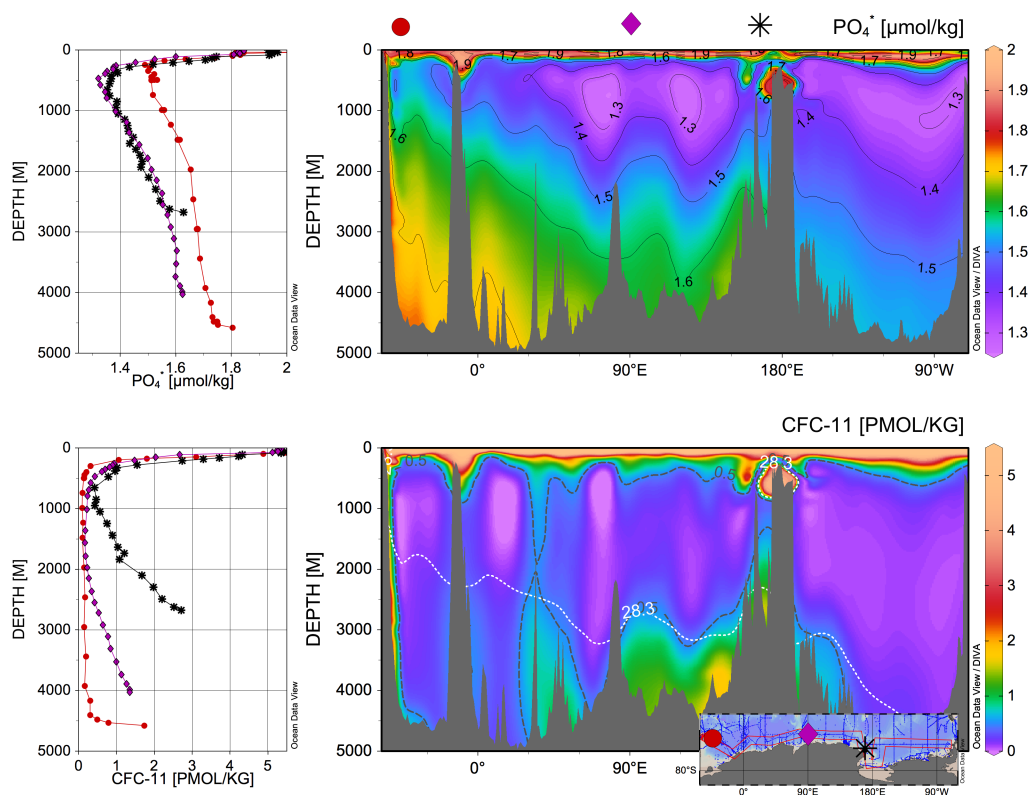


Figure 5. Circum Antarctic sections of PO_4^* and CFC-11 through the southern portion of the Southern Ocean. The locations of the profiles in the left hand panel are illustrated with symbols and shown in the inset map: the red circles are from the Weddell Sea, the purple diamonds from the Antarctic margin in the Indian sector, and the black stars from the northern margin of the Ross Sea. In the CFC section the black dashed line indicates CFC-11 concentrations >0.5 pmol/kg and the white dotted line indicates neutral densities >28.3 kg/m³; these criteria, along with depth >1500 m, are used to define the alternative deep Southern Ocean PO_4^* end member. Data are from GLODAPv2 (Key et al., 2015; Olsen et al., 2016) with profiles, maps, and sections plotted in ODV (Schlitzer 2015), with sections contoured using isopycnic gridding.

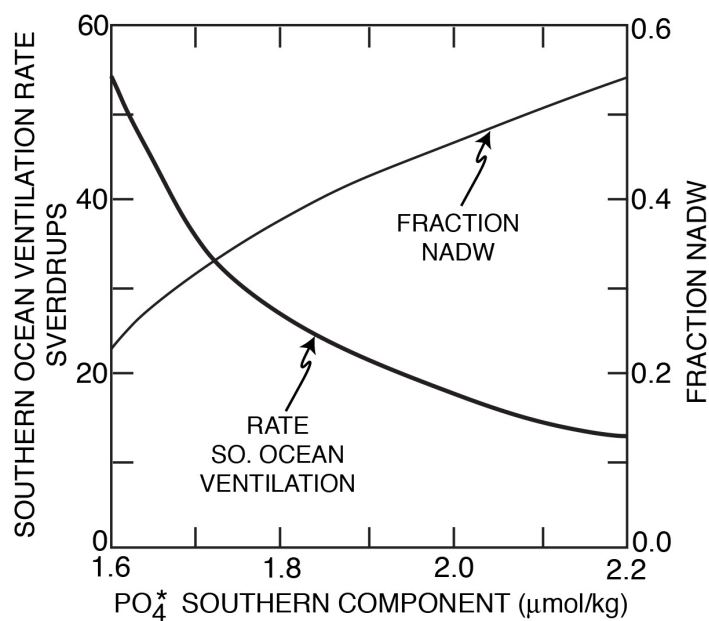


Figure 6. Rate of deep water formation in the deep Southern Ocean as a function of its concentration of PO_4^* . Also shown is the corresponding fraction of NADW in the water ventilating the deep Pacific and Indian Oceans. As 1.64 and 1.95 $\mu\text{mol/kg}$ represent reasonable limits for the PO_4^* value for deep waters formed in the Southern Ocean, the fraction of Pacific and Indian deep water supplied from the northern Atlantic could be anywhere from 23 to 54 percent.

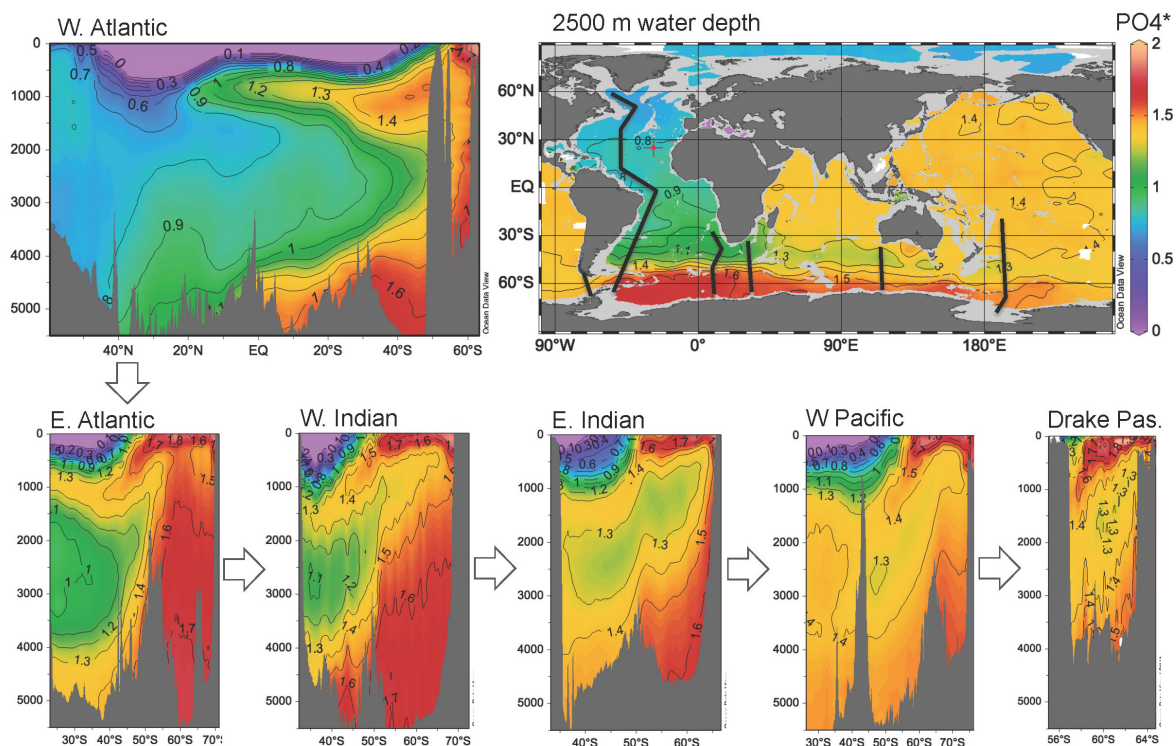


Figure 7. PO₄* sections for the western Atlantic and for a series of quadrants of the Southern Ocean. Low PO₄* waters entering the Southern Ocean from the Atlantic and the high PO₄* waters generated in the Southern Ocean are blended in the Antarctic Circumpolar Current, forming circumpolar deep water. However a PO₄* high at the seafloor and low at ~2000 m continue to trace the influence of AABW and NADW respectively. Data are from GLODAPv2 (Key et al., 2015; Olsen et al., 2016) with profiles, maps, and sections plotted in ODV (Schlitzer 2015), with sections contoured using isopycnal gridding.

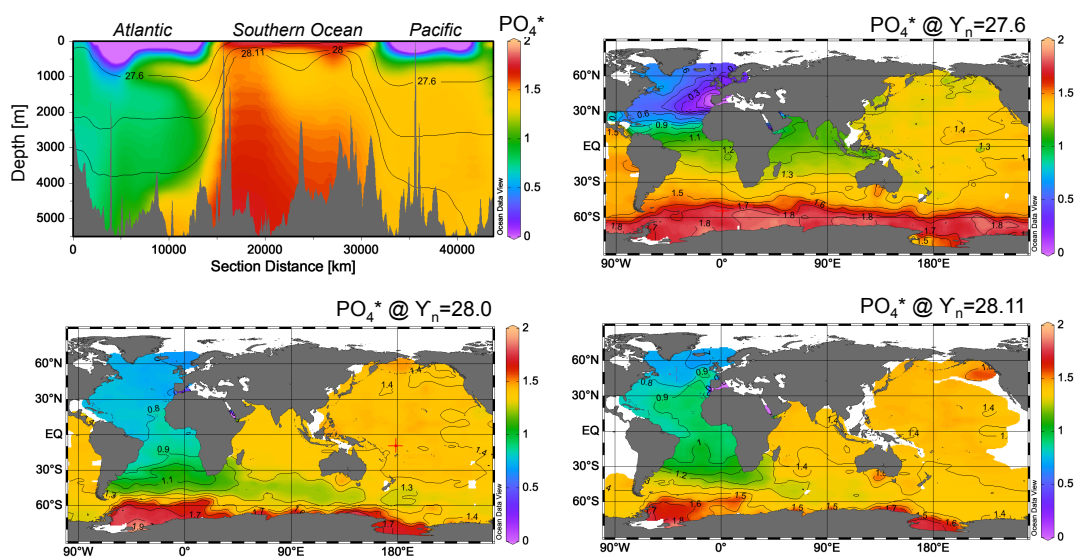


Figure 8. PO_4^* on a section through the Atlantic, Southern, and Pacific Oceans and on the 27.6, 28.0, and 28.11 isopycnal horizons. The depths of these horizons are shown in the section. Mixing of low PO_4^* from the North and high PO_4^* from the South takes place along shared isopycnals, and also diapycnally in the Southern Ocean mixed layer and over rough bottom topography. Data are from GLODAPv2 (Key et al., 2015; Olsen et al., 2016) with profiles, maps, and sections plotted in ODV (Schlitzer 2015).



References

- Abernathy, R. and Ferreira, D., 2015. Southern Ocean isopycnal mixing and ventilation changes driven by winds. *Geophysical Research Letters*, 42(23).
- Anderson, L.A. and Sarmiento, J.L., 1994. Redfield ratios of remineralization determined by nutrient data analysis. *Global biogeochemical cycles*, 8(1), pp.65-80.
- Barker, S., Diz, P., Vautravers, M.J., Pike, J., Knorr, G., Hall, I.R. and Broecker, W.S., 2009. Interhemispheric Atlantic seesaw response during the last deglaciation. *Nature*, 457(7233), pp.1097-1102.
- Broecker, W.S., Takahashi, T. and Takahashi, T., 1985. Sources and flow patterns of deep-ocean waters as deduced from potential temperature, salinity, and initial phosphate concentration. *Journal of Geophysical Research: Oceans*, 90(C4), pp.6925-6939.
- Broecker, W.S., Peng, T.H., Ostlund, G. and Stuiver, M., 1985. The distribution of bomb radiocarbon in the ocean. *Journal of Geophysical Research: Oceans*, 90(C4), pp.6953-6970.
- Broecker, W.S., Peacock, S., Walker, S., Weiss, R., Fahrbach, E., Schroeder, M., Mikolajewicz, U., Heinze, C., Carmack, E.C. and Foster, T.D., 1975, November. On the flow of water out of the Weddell Sea. In *Deep Sea Research and Oceanographic Abstracts* (Vol. 22, No. 11, pp. 711-724). Elsevier.
- Conkright, M.E., Boyer, T.P. and Levitus, S., 1994. *World Ocean Atlas: 1994 Nutrients* (Vol. 1). DIANE Publishing.
- Dong, S., Sprintall, J., Gille, S.T. and Talley, L., 2008. Southern Ocean mixed-layer depth from Argo float profiles. *Journal of Geophysical Research: Oceans*, 113(C6).
- England, M.H., 1995. Using chlorofluorocarbons to assess ocean climate models. *Geophysical Research Letters*, 22(22), pp.3051-3054.
- Ferrari, R., Jansen, M.F., Adkins, J.F., Burke, A., Stewart, A.L. and Thompson, A.F., 2014. Antarctic sea ice control on ocean circulation in present and glacial climates. *Proceedings of the National Academy of Sciences*, 111(24), pp.8753-8758.
- Key, R., Peng, T.-H., Rubin, S. 1998. How much deep water is formed in the Southern Ocean? *J. Geophys. Res.* 103, 15,833-15,843.
- Ganachaud, A. and Wunsch, C., 2000. Improved estimates of global ocean circulation, heat transport and mixing from hydrographic data. *Nature*, 408(6811), pp.453-457.
- Gebbie, G., Huybers, P. 2010. Total matrix intercomparison: A method for determining the geometry of water-mass pathways. *J. Phys. Oceanography* 40, 1710-1728.
- Gordon, A.L. and Huber, B.A., 1990. Southern Ocean winter mixed layer. *Journal of Geophysical Research: Oceans*, 95(C7), pp.11655-11672.
- Gouretski, V. and Koltermann, K.P., 2004. WOCE global hydrographic climatology. *Berichte des BSH*, 35, pp.1-52.



- Hupe, A. and Karstensen, J., 2000. Redfield stoichiometry in Arabian Sea subsurface waters. *Global Biogeochemical Cycles*, 14(1), pp.357-372.
- Johnson, G.C., 2008. Quantifying Antarctic bottom water and North Atlantic deep water volumes. *Journal of Geophysical Research: Oceans*, 113(C5).
- Key, R.M., Olsen, A., van Heuven, S., Lauvset, S.K., Velo, A., Lin, X., Schirnack, C., Kozyr, A., Tanhua, T., Hoppema, M. and Jutterström, S., 2015. Global Ocean Data Analysis Project, Version 2 (GLODAPv2).
- Khatiwala, S., Primeau, F., Holzer, M. 2012. Ventilation of the deep ocean constrained with tracer observations and implications for radiocarbon estimates of ideal mean age. *Earth Planet. Sci. Lett.* 325-326, 116-125.
- Lumpkin, R. and Speer, K., 2007. Global ocean meridional overturning. *Journal of Physical Oceanography*, 37(10), pp.2550-2562.
- Maier-Reimer, E. and Hasselmann, K., 1987. Transport and storage of CO₂ in the ocean—an inorganic ocean-circulation carbon cycle model. *Climate dynamics*, 2(2), pp.63-90.
- Marinov, I., Gnanadesikan, A., Toggweiler, J.R. and Sarmiento, J.L., 2006. The southern ocean biogeochemical divide. *Nature*, 441(7096), pp.964-967.
- Marshall, J. and Speer, K., 2012. Closure of the meridional overturning circulation through Southern Ocean upwelling. *Nature Geoscience*, 5(3), pp.171-180.
- Naveira-Garabato, A.C.N., Polzin, K.L., King, B.A., Heywood, K.J. and Visbeck, M., 2004. Widespread intense turbulent mixing in the Southern Ocean. *Science*, 303(5655), pp.210-213.
- Olsen, A., Key, R.M., van Heuven, S., Lauvset, S.K., Velo, A., Lin, X., Schirnack, C., Kozyr, A., Tanhua, T., Hoppema, M. and Jutterström, S., 2016. The Global Ocean Data Analysis Project version 2 (GLODAPv2)—an internally consistent data product for the world ocean. *Earth System Science Data*, 8(2), p.297.
- Orsi, A.H., Johnson, G.C. and Bullister, J.L., 1999. Circulation, mixing, and production of Antarctic Bottom Water. *Progress in Oceanography*, 43(1), pp.55-109.
- Orsi, A.H., Jacobs, S.S., Gordon, A.L. and Visbeck, M., 2001. Cooling and ventilating the abyssal ocean. *Geophysical Research Letters*, 28(15), pp.2923-2926.
- Orsi, A.H., Smethie, W.M. and Bullister, J.L., 2002. On the total input of Antarctic waters to the deep ocean: A preliminary estimate from chlorofluorocarbon measurements. *Journal of Geophysical Research: Oceans*, 107(C8).
- Peacock, S., Visbeck, M. and Broecker, W., 2000. Deep water formation rates inferred from global tracer distributions: An inverse approach. *Inverse Methods in Global Biogeochemical Cycles*, pp.185-195.
- Roemmich, D., Johnson, G.C., Riser, S., Davis, R., Gilson, J., Owens, W.B., Garzoli, S.L., Schmid, C. and Ignaszewski, M., 2009. The Argo Program: Observing the global ocean with profiling floats. *Oceanography*, 22(2), pp.34-43.



- Sarmiento, J.Á., Gruber, N., Brzezinski, M.A. and Dunne, J.P., 2004. High-latitude controls of thermocline nutrients and low latitude biological productivity. *Nature*, 427(6969), pp.56-60.
- Schlitzer, R., 2007. Assimilation of radiocarbon and chlorofluorocarbon data to constrain deep and bottom water transports in the world ocean. *Journal of Physical Oceanography*, 37(2), pp.259-276.
- Schlitzer, R., Ocean Data View, <http://odv.awi.de>, 2015.
- Schlosser, P., Bonisch, G., Rhein, M. and Bayer, R., 1991. Reduction of Deepwater Formation in the Greenland Sea during the 1980's. *Evidence from Tracer Data, Science*, 251, p.1054.
- Sigman, D.M., Hain, M.P. and Haug, G.H., 2010. The polar ocean and glacial cycles in atmospheric CO₂ concentration. *Nature*, 466(7302), pp.47-55.
- Sloyan, B.M. and Rintoul, S.R., 2001. The Southern Ocean limb of the global deep overturning circulation. *Journal of Physical Oceanography*, 31(1), pp.143-173.
- Smethie, W.M. and Fine, R.A., 2001. Rates of North Atlantic Deep Water formation calculated from chlorofluorocarbon inventories. *Deep Sea Research Part I: Oceanographic Research Papers*, 48(1), pp.189-215.
- Stocker, T.F. and Johnsen, S.J., 2003. A minimum thermodynamic model for the bipolar seesaw. *Paleoceanography*, 18(4).
- Takahashi, T., Broecker, W.S. and Langer, S., 1985. Redfield ratio based on chemical data from isopycnal surfaces. *Journal of Geophysical Research: Oceans*, 90(C4), pp.6907-6924.
- Talley, L.D., 1993. Distribution and formation of North Pacific intermediate water. *Journal of Physical Oceanography*, 23(3), pp.517-537.
- Talley, L.D., 1996. Antarctic intermediate water in the South Atlantic. *The South Atlantic: Present and Past Circulation*, pp.219-238.
- Talley, L.D., 2013. Closure of the global overturning circulation through the Indian, Pacific, and Southern Oceans: Schematics and transports. *Oceanography*, 26(1), pp.80-97.
- Toggweiler, J.R. and Samuels, B., 1995. Effect of Drake Passage on the global thermohaline circulation. *Deep Sea Research Part I: Oceanographic Research Papers*, 42(4), pp.477-500.
- Warren, B.A., 1981. Deep circulation of the world ocean. *Evolution of physical oceanography*, pp.6-41.

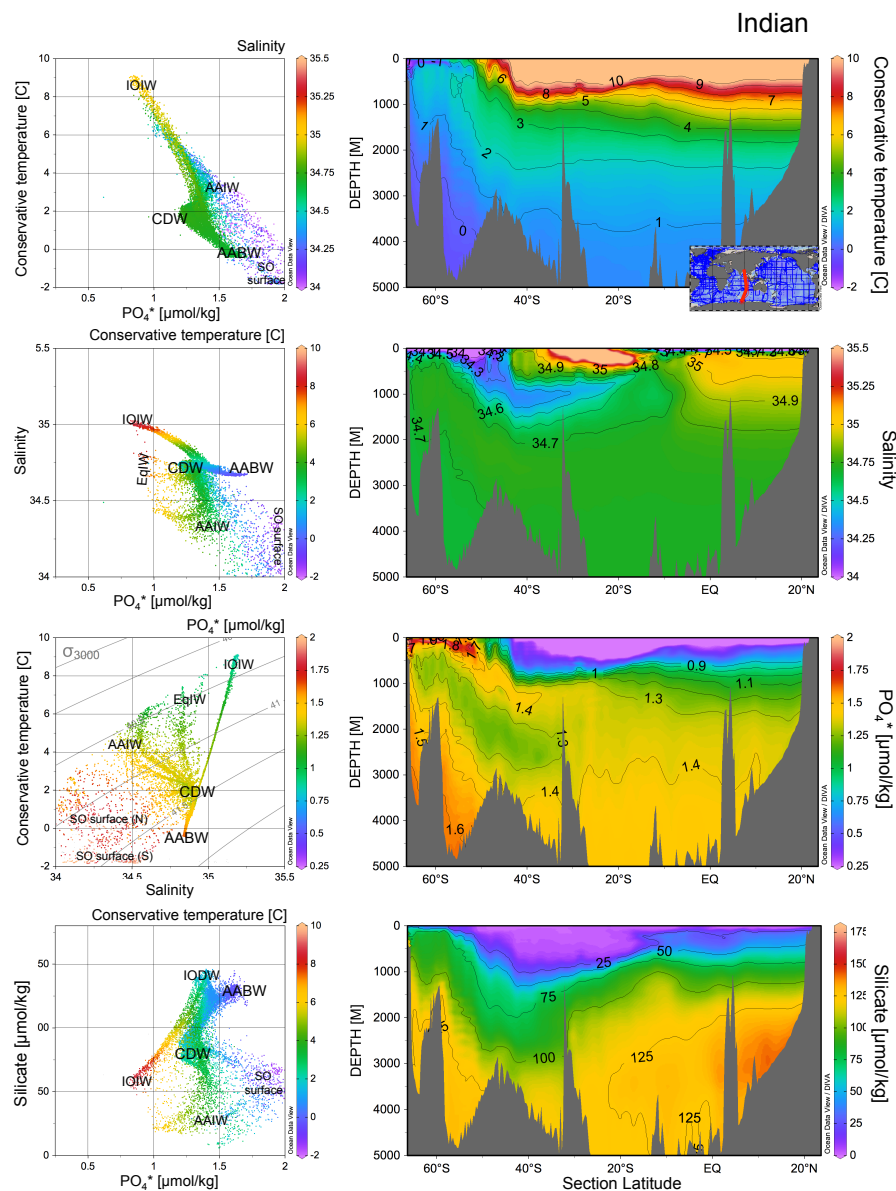


Figure A2: Indian Ocean hydrographic section for potential temperature, salinity, PO_4^* , and silicate. Cross plots show all the data in this section with neutral density greater than 27.2 kg/m^3 ; the colours of the dots refer to the scale shown to the right of the cross plots. Data are from GLODAPv2 (Key et al., 2015; Olsen et al., 2016) with profiles, maps, and sections plotted in ODV (Schlitzer 2015), with sections contoured using isopycnic gridding.

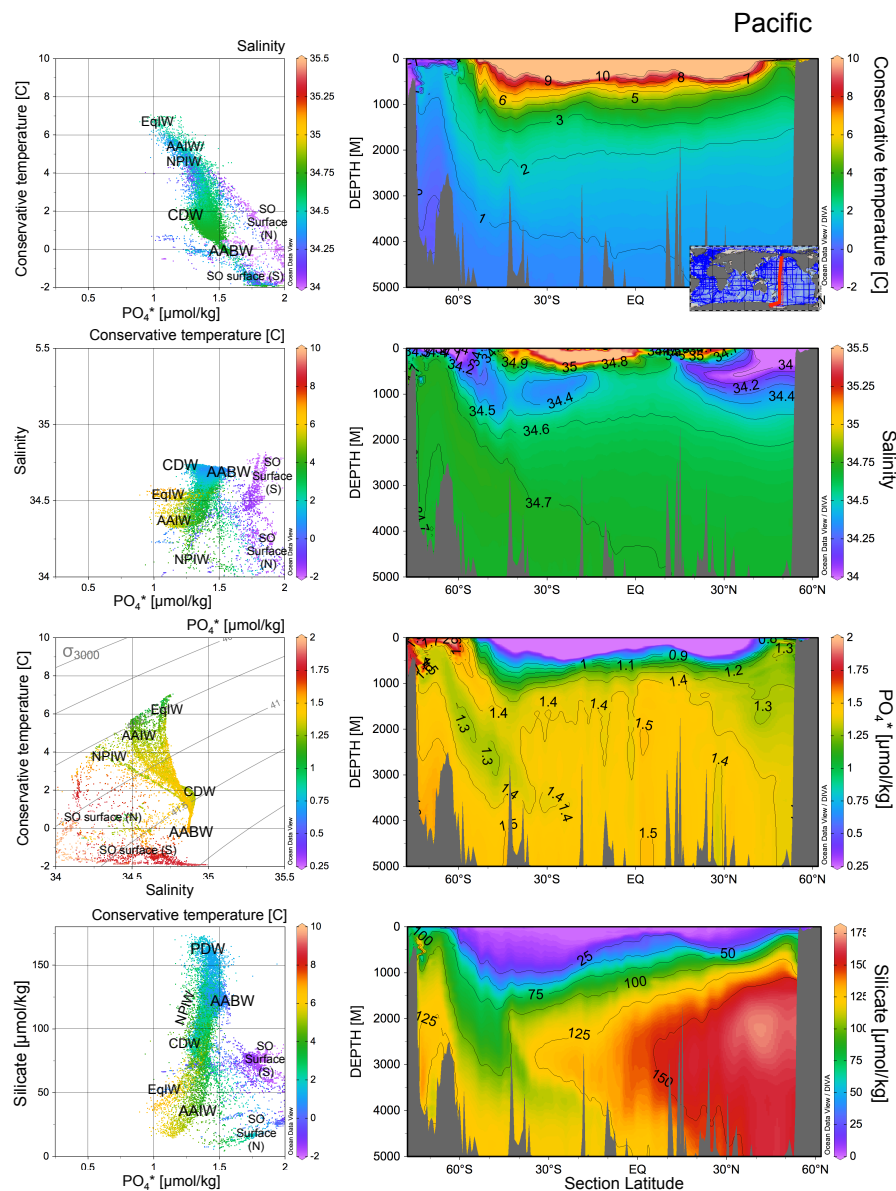


Figure A3: Pacific hydrographic section for potential temperature, salinity, PO_4^* , and silicate. Cross plots show all the data in this section with neutral density greater than 27.2 kg/m^3 ; the colours of the dots refer to the scale shown to the right of the cross plots. Data are from GLODAPv2 (Key et al., 2015; Olsen et al., 2016) with profiles, maps, and sections plotted in ODV (Schlitzer 2015), with sections contoured using isopycnic gridding.

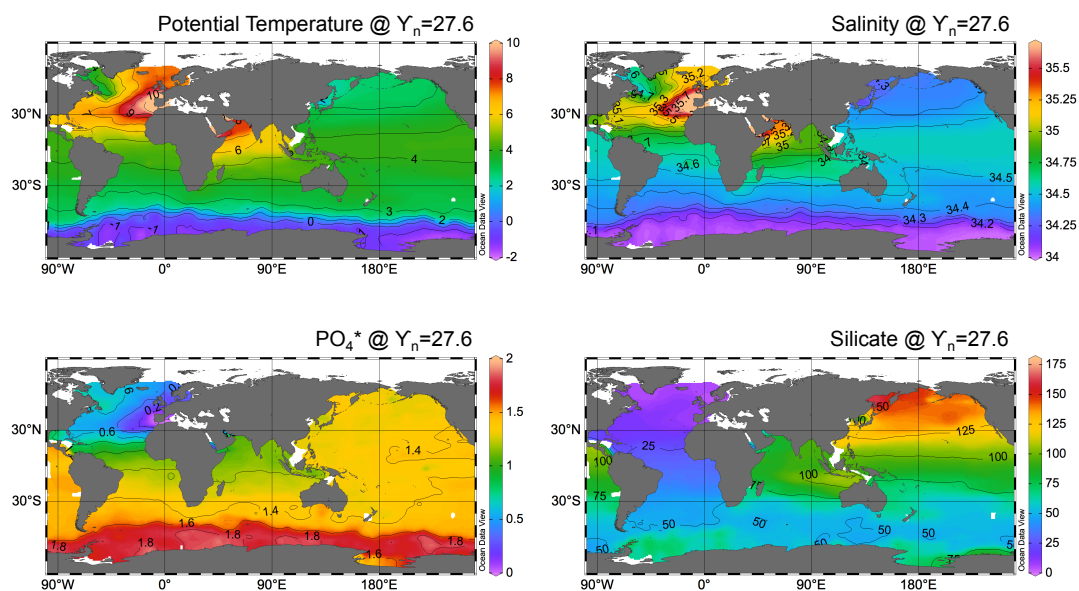


Figure A4: Potential temperature, salinity, PO_4^* , and silicate on the 27.6 isopycnal horizon. The depth of this horizon is shown in Figure 8 and averages ~ 1000 m in the basins and is in the mixed layer in the Southern Ocean. Data are from GLODAPv2 (Key et al., 2015; Olsen et al., 2016) with profiles, maps, and sections plotted in ODV (Schlitzer 2015).

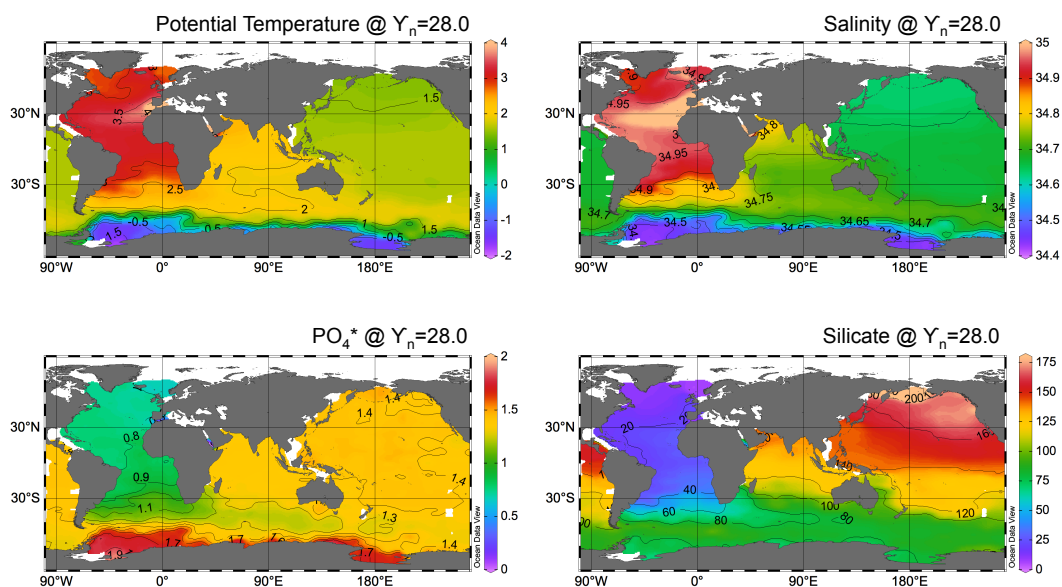


Figure A5: Potential temperature, salinity, PO_4^* , and silicate on the 28.0 isopycnal horizon. The depth of this horizon is shown in Figure 8 and averages ~ 2500 m in the basins and ~ 250 m in the mixed layer in the Southern Ocean. Data are from GLODAPv2 (Key et al., 2015; Olsen et al., 2016) with profiles, maps, and sections plotted in ODV (Schlitzer 2015).

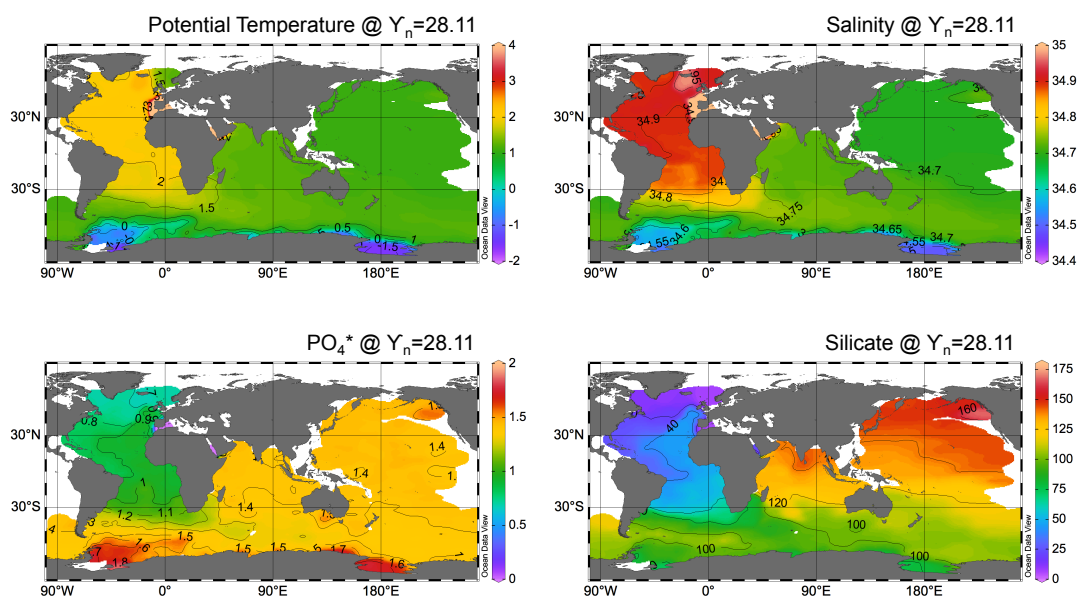


Figure A6: Potential temperature, salinity, PO_4^* , and silicate on the 28.3 isopycnal horizon. The depth of this horizon is shown in Figure 8 and averages ~ 4000 m in the basins and ~ 400 m in the mixed layer in the Southern Ocean. Data are from GLODAPv2 (Key et al., 2015; Olsen et al., 2016) with profiles, maps, and sections plotted in ODV (Schlitzer 2015).